Hindawi Publishing Corporation
Journal of Nanomaterials
Volume 2015, Article ID 573253, 7 pages
http://dx.doi.org/10.1155/2015/573253

Hindawi

Research Article

Upconversion Luminescence Properties of Y_2O_3:Yb, Er and Y_2O_2S:Yb, Er Nanoparticles Prepared by Complex Precipitation

Ying Tian,[1,2] Yao Fu,[1] Mingming Xing,[1] and Xixian Luo[1]

[1]*Optoelectronic Technology Institute, Dalian Maritime University, Dalian, Liaoning 116026, China*
[2]*NanoMaterials Group, Department of Applied Physics and Center for New Materials, Aalto University, 00076 Aalto, Finland*

Correspondence should be addressed to Ying Tian; ying.tian@aalto.fi and Xixian Luo; luoxixiandl@126.com

Received 8 December 2014; Revised 22 February 2015; Accepted 23 February 2015

Academic Editor: Gong-Ru Lin

The Yb^{3+}, Er^{3+} doped Y_2O_3 and Y_2O_2S upconversion nanophosphors were prepared by the direct complex precipitation method with the mixed solution of NH_4HCO_3 and $NH_3{\cdot}H_2O$ as the complex precipitant. The precipitate of $Re(OH)_x(CO_3)_y$ calcined at 900°C in air presents the pure Y_2O_3 with cubic structure, and the calculated crystalline size is about 26 nm, while the Y_2O_2S:Yb, Er nanocrystals were obtained by annealing the same precipitate at 900°C but in the atmosphere of N_2 gas containing sulfur vapor. The obtained sample presents the pure hexagonal structure of Y_2O_2S with calculated crystalline size of 29 nm. According to the transmission electronic microscopy (TEM), the nanophosphors exhibit uniform quasispherical shape and size about 30 nm. By using the 980 nm excitation laser, the properties of upconversion luminescence and energy transfer processes were studied in detail for the different concentration of Yb^{3+} in Er^{3+} doped Y_2O_3 as well as the Yb^{3+}, Er^{3+} codoped Y_2O_2S nanocrystals. The high-efficient red and yellow upconversion emissions were both observed by naked eyes in day time corresponding to the Y_2O_3:Yb, Er and Y_2O_2S:Yb, Er phosphors, respectively. Thus the upconversion nanoparticles combining its high efficient emission would pave the way for ideal fluorescence probes in biological applications.

1. Introduction

An upconversion process is one that takes multiple photons of lower energy and converts them to one photon of higher energy. There has been considerable research on the upconversion phosphor since it was found by Professor Auzel [1] for the first time and put forward being used in infrared detection and short-wave laser. More recently, people have found that if the upconversion phosphors can realize the nanocrystalline, combining its unique characteristics of luminescence, such as lack of background phosphorescence, no photobleaching during assay, and narrow emission bands [2, 3], it will have enormous potential applications in the areas of biomedical diagnosis [4], the anticounterfeiter [5], and display screen and X-ray imaging [6]. In particular, the Y_2O_3 and Y_2O_2S materials have attracted much interest as host materials for its excellent chemical stability, insoluble in water, high melting point, and low phonon energy [7–11]. Therefore, the high luminescence efficiency can be achieved in those systems via suitable selection of rare earth doping ions and excitation routes.

Many synthesis techniques of rare earth oxide and oxysulfide nanomaterials have been studied, such as precipitation method [12, 13], combustion synthesis [14], and emulsion liquid membrane system [15]. Among them, the precipitation method has become a promising chemical preparation rout owing to its advantages of simple process without complex equipment, easy doping, and low production cost. In particular, the homogeneous precipitation method has drawn a great attention in the fields of nanomaterial synthesis. Because the precipitants sedimentate out homogeneously and slowly in the solution, which accordingly conduce to the homogeneous formation of precipitates. And the obtained nanoparticles are uniform and fine in size [13, 16]. The urea ($CO(NH_2)_2$) as the precipitant has been most commonly used in the homogeneous precipitation method. However, the hydrolysis of urea is very slow process and need certain temperature. Moreover, the low concentration of urea is a necessity in order to obtain uniform nanoparticles; thus the big amount of reaction solution causes lots of difficulties in the posterior processes, such as filtration.

In the current work, the nanocrystalline upconversion phosphors were prepared by the direct complex precipitation method using the ammonium water and ammonium bicarbonate as the complex precipitants. This novel method makes use of the principal of homogeneous precipitation method but successfully overcomes the disadvantages of the urea homogeneous precipitation route. The Yb^{3+}, Er^{3+} codoped Y_2O_3 and Y_2O_2S upconversion nanophosphors are obtained with homogeneous morphology and meanwhile exhibit high efficient upconversion luminescence. The luminescence properties and mechanisms are discussed in detail for different host materials and doping concentrations.

2. Materials and Methods

2.1. Experiment Principles. In the complex precipitant solution of NH_4HCO_3 and $NH_3{\cdot}H_2O$, the equilibrium balances in the solution are shown as follows:

$$NH_4HCO_3 \longleftrightarrow NH_4^+ + HCO_3^- \quad (1)$$

$$HCO_3^- \longleftrightarrow H^+ + CO_3^{2-} \quad K_1 = 4.8 \times 10^{-11} \quad (2)$$

$$NH_3 \cdot H_2O \longleftrightarrow NH_4^+ + OH^- \quad K_2 = 1.79 \times 10^{-5} \quad (3)$$

$$H_2O \longleftrightarrow H^+ + OH^- \quad K_3 = 1 \times 10^{-14} \quad (4)$$

When the rare earth ions join in the reaction,

$$RE^{3+} + yCO_3^{2-} + xOH^- + nH_2O \longrightarrow RE(OH)_x(CO_3)_y \cdot H_2O \downarrow \quad (5)$$

Here K_1, K_2, and K_3 are the equilibrium constants of the three relevant reactions, respectively. Since the ammonium bicarbonate is strong electrolyte, the first reaction is a complete reaction. While the ammonium water and HCO_3^- both possess the properties of weak electrolytes, so that the quantity of the OH^- and CO_3^{2-} ions is little in the solution. When the complex precipitant solution of NH_4HCO_3 and $NH_3{\cdot}H_2O$ was dropped into the mixed solution of Y^{3+}, Yb^{3+}, and Er^{3+} ions, in the small area around the complex precipitants, the precipitants ionize out OH^- and CO_3^{2-} ions slowly according to the reversible reactions listed above. Then there is always little change of the OH^- and CO_3^{2-} concentrations within the small area, and the reversible reaction goes towards the positive direction with the formation of the precipitates. Namely, the concentration of the OH^- and CO_3^{2-} within the small area is correlative with the formation of precipitates. Therefore, the precipitation process is a local homogeneous process. When introducing the rare earth ions, the precipitates of carbonate $(Re(OH)_x(CO_3)_y$, where the Re represents Y, Yb, and Er) were formed by reacting with the OH^-, CO_3^{2-} ions simultaneously.

2.2. Materials Preparation. The certain amount of NH_4HCO_3 powders was dissolved into the $NH_3{\cdot}H_2O$ solution and then stirred vigorously to obtain the complex precipitant solution of 70 mL, and concentrations of the NH_4HCO_3 and $NH_3{\cdot}H_2O$ were 3 and 1 mol/L, respectively. The nitrate solutions of rare earth (Y_2O_3, Yb_2O_3, and Er_2O_3 powers (99.99%)) were weighed on the stoichiometry and mixed thoroughly, where the doped concentrations of the activator Er^{3+} were 0.8 mol%, and concentrations of the sensitizer Yb^{3+} were changed from 0 to 11 mol%. Then the complex precipitant solution was slowly dropped into the nitrate solution of rare earth that was vigorously stirred. The mixed solution was continuously stirred for 30 mins and then stayed for 2 hs. The resultant white precipitates of $Re(OH)_x(CO_3)_y$ were centrifuged and washed by water, ethanol, and acetone, respectively. The $Re(OH)_x(CO_3)_y$ precursor was finally dried at 60°C.

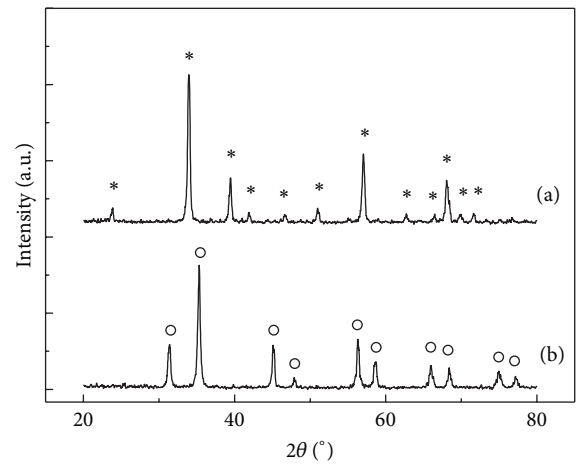

Figure 1: XRD patterns of (a) Y_2O_3:Yb, Er and (b) Y_2O_2S:Yb, Er nanocrystals calcined at 900°C (∗ and ○ denote the characteristic peaks corresponding to Y_2O_3 and Y_2O_2S, resp.).

Y_2O_3:Yb, Er nanophosphors were obtained by annealing the $Re(OH)_x(CO_3)_y$ precursor in air at 900°C for 1 h. While Y_2O_2S:Yb, Er nanophosphor was obtained by calcining the same $Re(OH)_x(CO_3)_y$ sample at 900°C for 1 h in the atmosphere of N_2 gas containing sulphur vapour, the sulphur vapour was generated by heating a sulfur powder at 400°C and then flowed into the tube by the N_2 gas.

2.3. Characterizations. X-ray diffraction (XRD) patterns of the samples were recorded on Hitachi DMAX-3A diffractometer equipped with $Co_{K\alpha}$ (λ = 0.15406 nm) radiation. The morphology of the sample was characterized by TEM (Tecnai G^2 20). The Hitachi F-4500 fluorescence spectrophotometer was utilized to measure the upconversion luminescence spectra. The excitation source was 980 nm laser diode (LD). The power of the LD was measured by the laser power meter (LPE-1 type).

3. Results and Discussions

3.1. Structure and Morphology. Figure 1 shows the XRD patterns of the samples that were calcined at 900°C in air and in N_2 gas containing sulfur vapor, respectively. The doping concentrations of Yb^{3+} and Er^{3+} ions of the two samples were

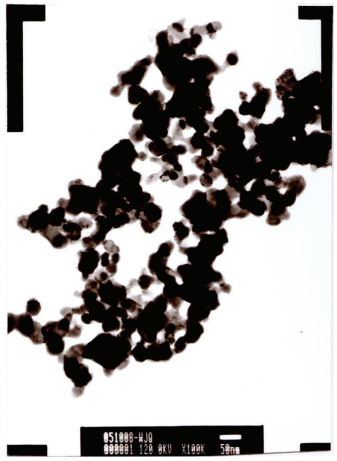

Figure 2: TEM image of the Y_2O_2S:Yb, Er phosphor annealed at 900°C.

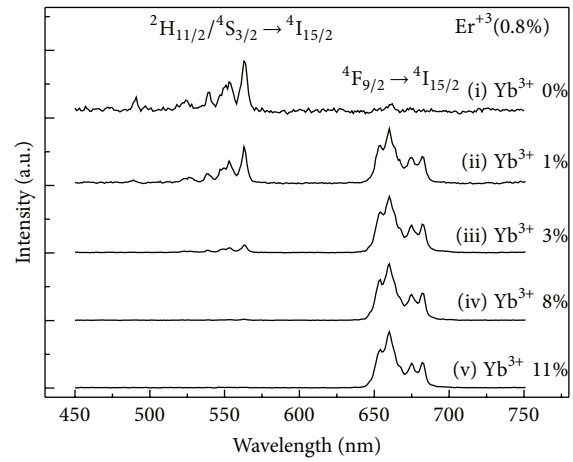

Figure 3: Upconversion spectra of the Er^{3+} (0.8 mol%), Yb^{3+} (0–11 mol%) codoped Y_2O_3 samples calcined at 900°C when excited by 980 nm LD.

both 8 and 0.8%. The results show that the sample calcined in air presents the pure Y_2O_3 phases with cubic structure, while the sample calcined in N_2 gas containing sulfur vapor exhibits the hexagonal structure of Y_2O_2S. Both of the patterns present pure Y_2O_3 and Y_2O_2S crystal structures without other phase. This result implies that the ions of Yb^{3+} and Er^{3+} have no influence on the crystal structure. And the as-prepared $Re(OH)_x(CO_3)_y$ powder obtained by the complex precipitation can be sulfurized thoroughly using the simple method of flowing N_2 gas containing the sulfur vapor. According to the Scherrer formula [17], $D = K\lambda/\beta\cos\theta$, the calculated crystallite size of theY_2O_3:Yb, Er and Y_2O_2S:Yb, Er particles was 26 and 29 nm, respectively.

For the observation of nanoparticles morphology, we loaded the Y_2O_2S:Yb, Er sample dispersed with ethanol on a TEM grid mesh. As shown in the TEM image (Figure 2), the obtained particles are in the quasispherical shape. Although some nanoparticles aggregate and form large particles, there are many well-dispersed nanoparticles around the agglomerates. Thus, it is feasible to observe the homogeneity of the particles as well as to evaluate the mean particle size. The assessed mean particle size from TEM image is about 30 nm, which exhibits a fairly good agreement with the calculated crystalline particle size on the basis of XRD measurement. In addition, the uniformity of the nanoparticles in both shape and size is achieved as shown in Figure 2, thereby indicating the promising advantages of the simple complex precipitation method.

3.2. Upconversion Luminescence Properties. Despite the ground bulk upconversion phosphors exhibit high luminescent efficiency, the big size and uneven morphology prevent their utilizations in the fields of biological applications as well as high-resolution displays. As suggested in the TEM measurements, the upconversion phosphors synthesized by the complex precipitation method reach to the high requirements of nanosize and homogeneity in both shape and size distribution. These features are ideal for the biological applications. Meanwhile, the very bright upconversion luminescence of the nanophosphors is observed by naked eyes when excited by LD with power as low as 5 mW. Figure 3 presents the upconversion emission spectra of the Er^{3+} (0.8 mol%), Yb^{3+} (0–11 mol%) codoped Y_2O_3 nanophorsphors by the excitation of 980 nm LD. The green and red emission bands at about 563 and 660 nm are assigned to the $^2H_{11/2}/^4S_{3/2} \rightarrow {}^4I_{15/2}$ and $^4F_{9/2} \rightarrow {}^4I_{15/2}$ intra-4f transitions of Er^{3+}, respectively. Upconversion luminescence is generally composed of ground state absorption (GSA), excited state absorption (ESA), energy transfer (ET), multiphonon relaxation, cross relaxation, and radiative transition [18]. Figure 3 (i) shows the upconversion luminescence spectrum of Y_2O_3:Er^{3+} (Er: 0.8 mol%) sample. The excitation wavelength matches the absorption transition between the ground state $^4I_{15/2}$ and excited level $^4I_{11/2}$. After the first-level excitation, two mechanisms are considered as follows [19]. One route is the simple ESA, where the same energy photons are absorbed by the excited state Er^{3+} ion from the $^4I_{11/2}$ to the $^4F_{7/2}$ level. The other route is ETU (energy transfer upconversion), where a mutual interaction between two excited Er^{3+} ($^4I_{11/2}$) may occur, with the results of one ion deexcited to $^4I_{15/2}$ while the other ion is excited to $^4F_{7/2}$ level. The above two upconversion mechanisms can both populate the $^4F_{7/2}$ state which then decays nonradiatively to the $^2H_{11/2}/^4S_{3/2}$ and $^4F_{9/2}$ levels, subsequently emitting green and red luminescence when returning to the ground state $^4I_{15/2}$, respectively. Due to the low doping concentration of Er^{3+} ion in the Y_2O_3:Er^{3+} sample, it was considered that the probability of occurring the first ESA mechanism is much more than the ETU mechanism between two Er^{3+} ions.

Figure 3 (ii)–(v) show the upconversion spectra of different concentration of Yb^{3+} in Er^{3+} doped Y_2O_3 nanocrystals under 980 nm LD excitation. It can be seen from the spectra that the relative intensity ratio I_r/I_g (I_r and I_g represent the red and green emission, resp.) rapidly increases with increasing the Yb^{3+} concentration, where the Yb^{3+} ions obviously

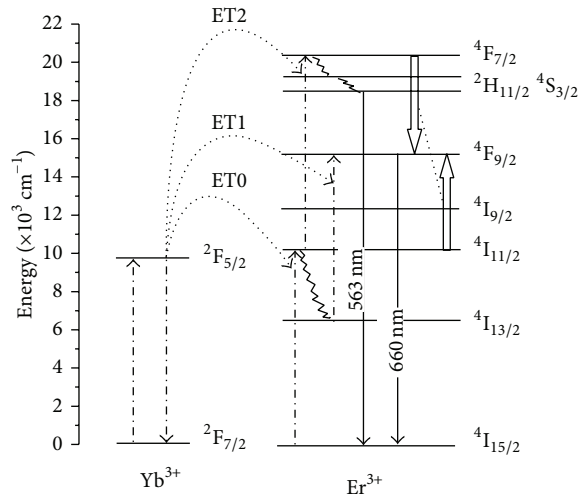

FIGURE 4: Schematic energy level diagram of Yb^{3+} and Er^{3+} ions under excitation of 980 nm LD.

play an important role. Since the Yb^{3+} ion has a much higher absorption cross-section than that of Er^{3+} ion at 980 nm [20], the roles that the Er^{3+} ion plays in the population of the excitation levels decrease with the increasing of the Yb^{3+} concentration.

As shown in the energy level diagram (Figure 4), the upconversion green and red emission mechanisms of the Y_2O_3:Yb, Er samples are analyzed as follows.

The upconversion channel of green luminescence (1) is as follows:

(1) $Yb^{3+}(^2F_{5/2}) + Er^{3+}(^4I_{15/2}) \rightarrow Yb^{3+}(^2F_{7/2}) + Er^{3+}(^4I_{11/2})$;

$Er^{3+}(^4I_{11/2}) + Yb^{3+}(^2F_{5/2}) \rightarrow Yb^{3+}(^2F_{7/2}) + Er^{3+}(^4F_{7/2}) \sim \cdot \sim Er(^4S_{3/2}/^2H_{11/2})$ ($\sim \cdot \sim$ denotes the process of multiphonons relaxation).

The $^4F_{7/2}$ state of Er^{3+} is populated via the twice energy transfer of channel (1), after nonradiative relaxation to the $^4S_{3/2}/^4H_{11/2}$ levels and then returns to the ground state emitting the upconversion green luminescence via radiation transition.

The upconversion channels of red luminescence (2), (3), and (4) are as follows:

(2) after the population of 4S3/2 level by channel (1), $Er(^4S_{3/2}) \sim \cdot \sim Er(^4F_{9/2})$ occur;

(3) $Er^{3+}(^4F_{7/2}) + Er^{3+}(^4I_{11/2}) \rightarrow 2Er^{3+}(^4F_{9/2})$;

(4) $Yb^{3+}(^2F_{5/2}) + Er^{3+}(^4I_{15/2}) \rightarrow Yb^{3+}(^2F_{7/2}) + Er^{3+}(^4I_{11/2}) \sim \cdot \sim Er^{3+}(^4I_{13/2})$;

$Yb^{3+}(^2F_{5/2}) + Er^{3+}(^4I_{13/2}) \rightarrow Yb^{3+}(^2F_{7/2}) + Er^{3+}(^4F_{9/2})$.

One can see that, three channels are involved in populating the excited state $^4F_{9/2}$ of Er^{3+} ion, that is, multiphonons relaxation from $^4S_{3/2}$ level, cross-relaxation process between Er^{3+} ions, and the $^4I_{13/2}$ level (Er^{3+}) reabsorbing the energy from excited state $^2F_{5/2}$ (Yb^{3+}) to further populate the $^4F_{9/2}$ level via the process of ET1, as shown in Figure 4.

It is well known that the increase of concentration of Yb^{3+} in Er^{3+} doped nanocrystals should greatly promote the ET from Yb^{3+} ($^2F_{5/2}$) to Er^{3+} ($^4I_{11/2}$) [21]. Thus more Er^{3+} will be excited to the $^4I_{11/2}$ level by the ET0, and correspondingly more Er^{3+} will be excited to the $^4F_{7/2}$ state with the increase of the population of $^4I_{11/2}$ through ET2 as shown in Figure 4. According to (i) (see [22]),

$$P \propto N_0 N_1, \tag{i}$$

where P is the cross-relaxation probability, N_0, N_1 are the population densities of the two states which are involved in the cross-relaxation process. Therefore, the cross-relaxation probability between the $^4I_{11/2}$ and $^4F_{7/2}$ levels increased greatly with the increase of Yb^{3+} concentration. This directly contributes to the population of the $^4F_{9/2}$ level to a large extent. Additionally, the population increase of the $^4I_{11/2}$ state will also result in the decay of Er^{3+} ions from $^4I_{11/2}$ to $^4I_{13/2}$ level; thus the process of ET1 is enhanced due to the increasing of population densities of Er^{3+} ($^4I_{13/2}$) and Yb^{3+} ($^2F_{5/2}$) ions. This also contributes to the population of $^4F_{9/2}$ level. Therefore, the occurrence probabilities of channels (3) and (4) both increase with the increase of Yb^{3+} concentration, which consequently result in the enhancement of population of $^4F_{9/2}$ level. As observed in Figure 3, the relative intensity ratio I_r/I_g increases gradually with the Yb^{3+} concentration increasing from 0 to 11%.

The pump mechanism can be studied by the relationship between the upconversion emission intensity and pump power; that is,

$$I_{\text{vis}} \propto \left(I_p\right)^n, \tag{ii}$$

where I_{vis} is the intensity of the upconversion emission, I_p is pump power, and n is the number of pump-photons required to populate the emitting state [23]. In order to confirm the upconversion mechanism discussed above, the intensity of green (563 nm) and red (660 nm) emission is measured as a function of pump power in three samples of Y_2O_3:0.8% Er, Y_2O_3:1% Yb, 0.8% Er, and Y_2O_3:11% Yb, 0.8% Er, as plotted in Figure 5. For the sample of Y_2O_3:Er, the slope corresponding to the emission intensities of the transitions $^2H_{11/2}/^4S_{3/2} \rightarrow {}^4I_{15/2}$ and $^4F_{9/2} \rightarrow {}^4I_{15/2}$ is both approximately 2. This indicates that generation of these transitions is predominantly due to two-photon absorption by Er^{3+}. For the sample of Y_2O_3:1% Yb, 0.8% Er, the slope values are slightly smaller than 2, which shows the upconversion mechanism is two-photon process but including some cross-relaxation and the ET processes from Yb^{3+} to Er^{3+} [23]. For the sample of Y_2O_3:11% Yb, 0.8% Er, the slope values are even smaller than that in the Y_2O_3:1% Yb, 0.8% Er sample, which implies that the upconversion mechanism must include more cross-relaxation and the ET processes from Yb^{3+} to Er^{3+}. These results further confirm the upconversion mechanism stated above.

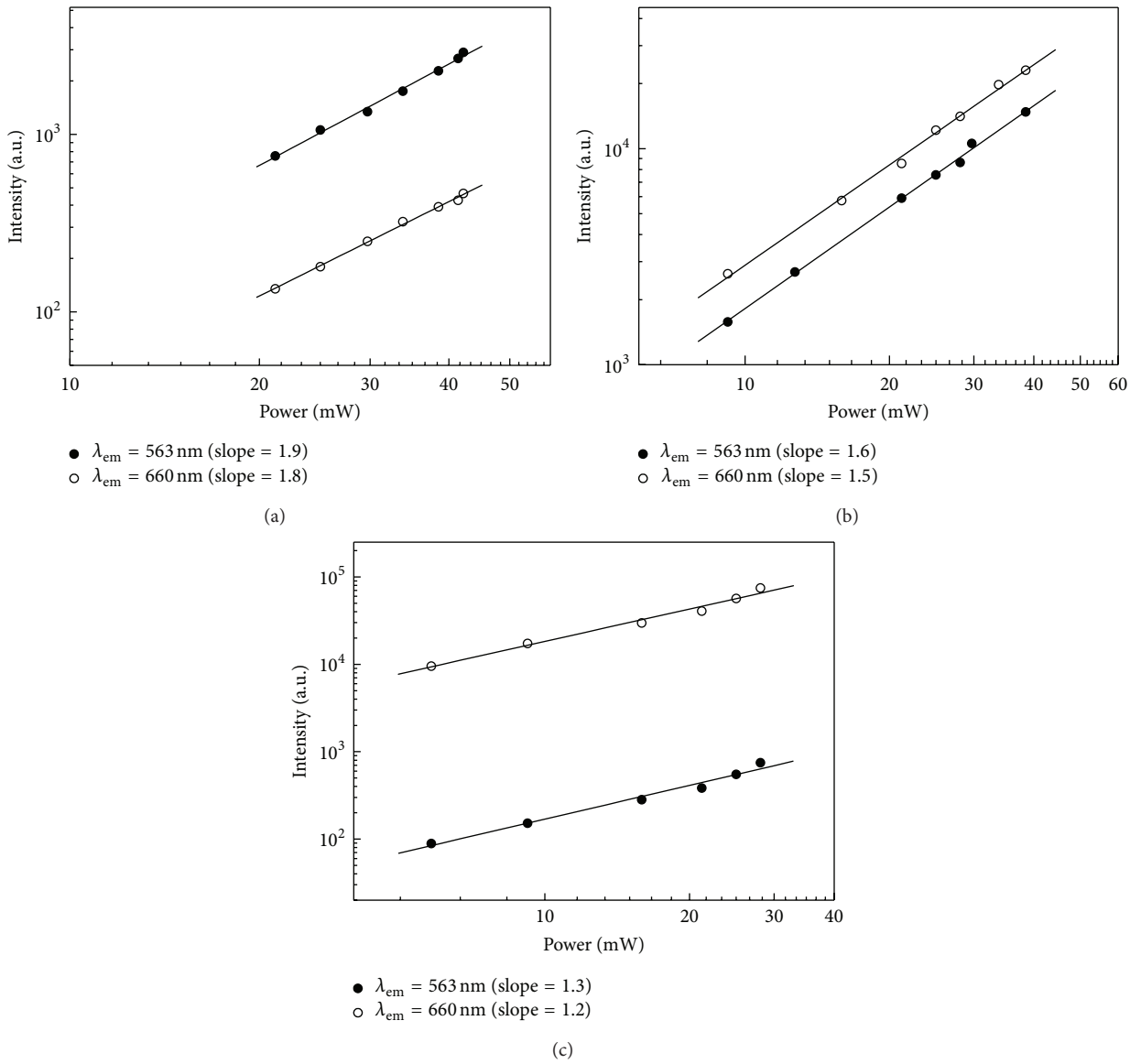

Figure 5: The upconversion emission intensity as a function of pump power for the three samples: (a) Y_2O_3:0.8% Er, (b) Y_2O_3:1% Yb, 0.8% Er, and (c) Y_2O_3:11% Yb, 0.8% Er.

Figure 6 shows the upconversion spectra of Y_2O_3:Yb, Er and Y_2O_2S:Yb, Er nanocrystal samples by the 980 nm LD excitation, and the doping concentrations of Yb^{3+} and Er^{3+} in the two samples are the same about 8 and 0.8%, respectively. Although the main peaks in the spectra are both red emission arising $^4F_{9/2} \rightarrow {}^4I_{15/2}$ transition of Er^{3+}, there are still some differences between them. The maximum of red emission peak of the Y_2O_3:Yb, Er sample is located at 660 nm; moreover, the green luminescence is almost quenched comparing with the intensity of red emission. When excited by LD only with the power of 5 mW, the upconversion red luminescence can be seen by naked eyes in the daytime. While in the spectrum of Y_2O_2S:Yb, Er sample, the maximum of red emission peak (668 nm) shifts to longer wavelength about 8nm when compared with that of yttrium oxide sample, and the green emission is enhanced to a certain extent. Similarly, under the excitation of 980 nm LD with power of 5 mW, the upconversion luminescence also can be seen in the daytime but appearing yellow to the naked eyes.

The phosphors of Y_2O_3 and Y_2O_2S come from the same precursor $Re(OH)_x(CO_3)_y$ sample, and the heat treatment, doping concentration, and measure conditions are all the same, so it is believed that the obvious differences between the two spectra must be related to the different host. As the intrinsic phonon energies of Y_2O_3 and Y_2O_2S are 597 and 520 cm^{-1}, respectively [24, 25], Y_2O_3 obviously possesses much higher phonon energy. So the probability of phonon-assisted nonradiative relaxation of $^4S_{3/2} \rightarrow {}^4F_{9/2}$ and $^4I_{11/2} \rightarrow {}^4I_{13/2}$ is much larger in Y_2O_3 host, which lead to the more effectively bypass or quench the green-light emitting states, as shown in Figure 6.

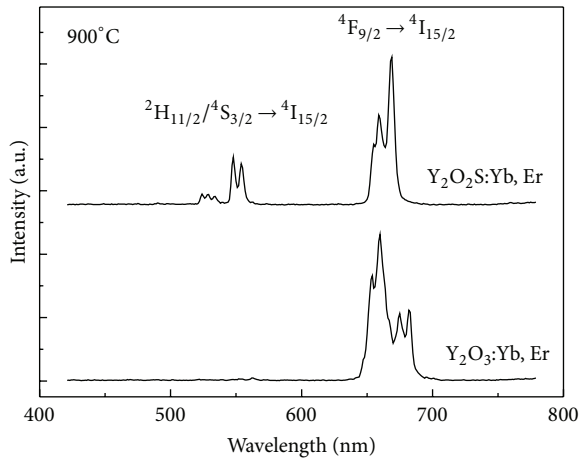

Figure 6: The upconversion spectra of Er^{3+} (0.8 mol%), Yb^{3+} (8 mol%) codoped Y_2O_2S and Y_2O_3 samples under the 980 nm excitation.

As compared with the Y_2O_3:Yb, Er samples, in the spectrum of Y_2O_2S:Yb, Er nanocrystals, the red shift of the main peak may be caused by the nephelauxetic effect in the system composed by the sulphured compounds [16]. Since the Er^{3+} ion is surrounded by the sulfur in the oxysulfide, this increases the covalent interaction in the system and shifts the transitions to smaller energies compared with the yttrium oxide. Pires has observed similar phenomenon in the Eu^{3+} doped oxysulfide system, that is, the emission peak arising from the $^5D_0 \rightarrow {}^7F_2$ transition of Eu^{3+} red shifts 14 nm in the oxysulfide compared with the oxide. The differences in the peak shape may be correlative to the crystal structure of the host crystal. When changing the crystal structure from cubic into hexagonal structure (from oxide to oxysulfide), the variation of the crystal-field surrounding the Er^{3+} ion may lead to the differences in the peak width and splitting mode.

4. Conclusions

The Y_2O_3:Yb, Er and Y_2O_2S:Yb, Er upconversion phosphor nanoparticles with crystallite size of 26 and 29 nm have been successfully prepared by the complex precipitation method by using the mixed solution of NH_4HCO_3 and $NH_3 \cdot H_2O$ as the complex precipitant, and the two samples present the pure cubic and hexagonal structure, respectively. For the Y_2O_3:Yb, Er sample, when keeping the Er^{3+} concentration a constant (0.8 mol%), the ratio I_r/I_g has increased greatly with the increase of Yb^{3+} concentration from 0 to 11 mol%. This could be attributed to the ET between rare earth ions and the cross-relaxation processes. In addition, the upconversion emission spectra of the two samples before and after sulphuration are different from each other. This may be correlated to the crystal structure and the intrinsic properties of different host crystals. It is worthy pointing out that the high efficient upconversion luminescence from the Y_2O_3:8% Yb, 0.8% Er and Y_2O_2S:Yb 8%, 0.8% Er phosphors can be seen by naked eyes in daytime when excited by the 980 nm LD with power as low as 5 mW. Therefore, these up-converting phosphor nanoparticles, with excellent luminescence properties, may become ideal fluorescence probes in the biochip technology and may be utilized as the anticounterfeiter and display screen materials.

Conflict of Interests

The authors declare that there is no conflict of interests regarding the publication of this paper.

Acknowledgments

The authors thank the New Century Educational Talent Plan of Chinese Education Ministry (NCET-10- 0171), Fundamental Research Funds for the Central Universities (3132015139, 3132015150, 3132015153, and 3132014327), Foundation of Liaoning Educational Committee (L2013201, L2014208, and L2014212), and Liaoning Excellent Talents in University (LR2013020).

References

[1] F. Auzel, "Computeur quantique par transfer d'energie de Yb^{3+}, Tm^{3+} dans un tungstate mixte et dans un verre gemanate," *Compte Rendus de l'Acadmie des Sciences*, vol. 263, pp. 819–821, 1966.

[2] J. Hampl, M. Hall, N. A. Mufti et al., "Upconverting phosphor reporters in immunochromatographic assays," *Analytical Biochemistry*, vol. 288, no. 2, pp. 176–187, 2001.

[3] H. J. M. A. A. Zijlmans, J. Bonnet, J. Burton et al., "Detection of cell and tissue surface antigens using up-converting phosphors: a new reporter technology," *Analytical Biochemistry*, vol. 267, no. 1, pp. 30–36, 1999.

[4] J. Liao, Z. Yang, S. Lai et al., "Upconversion emission enhancement of $NaYF_4$:Yb,Er nanoparticles by coupling silver nanoparticle plasmons and photonic crystal effects," *The Journal of Physical Chemistry C*, vol. 118, no. 31, pp. 17992–17999, 2014.

[5] J. Zhang, H. Zhao, X. Zhang et al., "Monochromatic Near-infrared to near-infrared upconversion nanoparticles for high-contrast fluorescence imaging," *Journal of Physical Chemistry C*, vol. 118, no. 5, pp. 2820–2825, 2014.

[6] Y. Liu, K. Ai, and L. Lu, "Designing lanthanide-doped nanocrystals with both up- and down-conversion luminescence for anti-counterfeiting," *Nanoscale*, vol. 3, no. 11, pp. 4804–4810, 2011.

[7] J. Silver, M. I. Martinez- Rubio, S. Gebretensae, G. R. Fern, M. J. Snowden, and R. Withnall, "A novel synthetic method for the controlled production of particle desired size for Y_2O_3:Eu phosphor using copolymer microgels of NIPAM," *SID Digest*, vol. 33, pp. 393–396, 2002.

[8] R. Withnall, J. Silver, T. G. Ireland, A. Lipman, G. R. Fern, and P. Saxty, "A new oxide/oxysulfide based phosphor triad and high-efficiency green- emitting $(Y,Gd)_2O_2S$:Tb phosphor for FED applications," *SID Digest*, vol. 36, pp. 594–597, 2005.

[9] X. Yan, G. R. Fern, R. Withnall, and J. Silver, "Contrasting behaviour of the co-activators in the luminescence spectra of $Y_2O_2S:Tb^{3+},Er^{3+}$ nanometre sized particles under UV and red light excitation," *Nanoscale*, vol. 5, no. 3, pp. 1091–1096, 2013.

[10] X. Yan, G. R. Fern, R. Withnall, and J. Silver, "Effects of the host lattice and doping concentration on the colour of Tb^{3+}

cation emission in $Y_2O_2S:Tb^{3+}$ and $Gd_2O_2S:Tb^{3+}$ nanometer sized phosphor particles," *Nanoscale*, vol. 5, no. 18, pp. 8640–8646, 2013.

[11] J. Silver, X. Yan, G. R. Fernand, and N. Wilkinson, "Cathodoluminescence spectra of single Y2O2S:Tb3+ nanometer sized phosphor crystals excited in a field emission scanning transmission electron microscope," in *Proceedings of the International Display Workshops (IDW '13)*, vol. 13, pp. 823–826, 2013.

[12] L. Li, W. Xiaochun, W. Xiantao, C. Yonghu, G. Changxin, and Y. Min, "Influence of precipitant solution pH on the structural, morphological and upconversion luminescent properties of Lu_2O_3:2%Yb, 0.2%Tm nanopowders," *Physica B: Condensed Matter*, vol. 406, no. 3, pp. 609–613, 2011.

[13] J. Silver, M. I. Martinez-Rubio, T. G. Ireland, G. R. Fern, and R. Withnall, "The effect of particle morphology and crystallite size on the upconversion luminescence properties of erbium and ytterbium co-doped yttrium oxide phosphors," *Journal of Physical Chemistry B*, vol. 105, no. 5, pp. 948–953, 2001.

[14] T. Xia, W.-H. Cao, X.-X. Luo, and Y. Tian, "Combustion synthesis and spectra characteristic of $Gd_2O_2S:Tb^{3+}$ and $La_2O_2S:Eu^{3+}$ x-ray phosphors," *Journal of Materials Research*, vol. 20, no. 9, pp. 2274–2278, 2005.

[15] T. Hirai and T. Orikoshi, "Preparation of Gd_2O_3:Yb,Er and Gd_2O_2S:Yb,Er infrared-to-visible conversion phosphor ultrafine particles using an emulsion liquid membrane system," *Journal of Colloid and Interface Science*, vol. 269, no. 1, pp. 103–108, 2004.

[16] A. M. Pires, M. R. Davolos, and E. B. Stucchi, "Eu^{3+} as a spectroscopic probe in phosphors based on spherical fine particle gadolinium compounds," *International Journal of Inorganic Materials*, vol. 3, no. 7, pp. 785–790, 2001.

[17] R. A. Spurr and H. Myers, "Quantitative analysis of anatase-rutile mixtures with an X-ray diffractometer," *Analytical Chemistry*, vol. 29, no. 5, pp. 760–762, 1957.

[18] J. Li, H. Hu, S. Li, and F. Gan, "The study of energy transfer and upconversion emmssion of Yb3+ /Er3+ co-doped tungsten-tellu-rite glasses," *Journal of the Chinese Ceramic Society*, vol. 31, pp. 1003–1006, 2003.

[19] D. Matsuura, H. Hattori, and A. Takano, "Upconversion luminescence properties of Y_2O_3 nanocrystals doped with trivalent rare-earth ions," *Journal of the Electrochemical Society*, vol. 152, no. 3, pp. H39–H42, 2005.

[20] F. Vetrone, J.-C. Boyer, J. A. Capobianco, A. Speghini, and M. Bettinelli, "Significance of Yb^{3+} concentration on the upconversion mechanisms in codoped $Y_2O_3:Er^{3+}$, Yb^{3+} nanocrystals," *Journal of Applied Physics*, vol. 96, no. 1, pp. 661–667, 2004.

[21] D. Matsuura, "Red, green, and blue upconversion luminescence of trivalent-rare-earth ion-doped Y_2O_3 nanocrystals," *Applied Physics Letters*, vol. 81, no. 24, pp. 4526–4528, 2002.

[22] X.-L. Yang, S.-G. Xiao, and Z.-W. Liu, "The study of upconversion fluorescence in Er^{3+}:Yb^{3+} co-doped oxy-fluoride glasses," *Spectroscopy and Spectral Analysis*, vol. 122, pp. 357–359, 2002.

[23] F. E. Auzel, "Materials and devices using double-pumped-phosphors with energy transfer," *Proceedings of the IEEE*, vol. 61, no. 6, pp. 758–786, 1973.

[24] G. F. J. Garlick and C. L. Richards, "Studies of the red anti-stokes emission of erbium ions in the Y_2O_2S: Er, Yb phosphor system," *Journal of Luminescence*, vol. 9, no. 5, pp. 432–439, 1974.

[25] J. A. Capobianco, P. Kabro, F. S. Ermeneux, R. Moncorgé, M. Bettinelli, and E. Cavalli, "Optical spectroscopy, fluorescence dynamics and crystal-field analysis of Er^{3+} in YVO_4," *Chemical Physics*, vol. 214, no. 2-3, pp. 329–340, 1997.